WATER RESOURCES RESEARCH, VOL. 30, NO. 3, PAGES 721–733, MARCH 1994

Water and heat fluxes in desert soils
2. Numerical simulations

Bridget R. Scanlon
Bureau of Economic Geology, University of Texas at Austin

P. C. D. Milly
U.S. Geological Survey, Geophysical Fluid Dynamics Laboratory/NOAA, Princeton, New Jersey

Abstract. Transient one-dimensional fluxes of soil water (liquid and vapor) and heat in response to 1 year of atmospheric forcing were simulated numerically for a site in the Chihuahuan Desert of Texas. The model was initialized and evaluated using the monitoring data presented in a companion paper (Scanlon, this issue). Soil hydraulic and thermal properties were estimated a priori from a combination of laboratory measurements, models, and other published information. In the first simulation, the main drying curves were used to describe soil water retention, and hysteresis was ignored. Remarkable consistency was found between computed and measured water potentials and temperatures. Attenuation and phase shift of the seasonal cycle of water potentials below the shallow subsurface active zone (0.0- to 0.3-m depth) were similar to those of temperatures, suggesting that water potential fluctuations were driven primarily by temperature changes. Water fluxes in the upper 0.3 m of soil were dominated by downward and upward liquid fluxes that resulted from infiltration of rain and subsequent evaporation from the surface. Upward flux was vapor dominated only in the top several millimeters of the soil during periods of evaporation. Below a depth of 0.3 m, water fluxes varied slowly and were dominated by downward thermal vapor flux that decreased with depth, causing a net accumulation of water. In a second simulation, nonhysteretic water retention was instead described by the estimated main wetting curves; the resulting differences in fluxes were attributed to lower initial water contents (given fixed initial water potential) and unsaturated hydraulic conductivities that were lower than they were in the first simulation. Below a depth of 0.3 m, the thermal vapor fluxes dominated and were similar to those in the first simulation. Two other simulations were performed, differing from the first only in the prescription of different (wetter) initial water potentials. These three simulations yielded identical solutions in the upper 0.2 m of soil after infiltration of summer rain; however, the various initial water potentials were preserved throughout the year at depths greater than 0.2 m. Comparison of all four simulations showed that the predominantly upward liquid fluxes below a depth of 0.2 m were very sensitive to the differences in water retention functions and initial water potentials among simulations, because these factors strongly affected hydraulic conductivities. Comparison of numerical modeling results with chemical tracer data showed that values of downward vapor flux below the surface evaporation zone were of the same order of magnitude as those previously estimated by analysis of depth distributions of bomb ^{3}H (volatile) and bomb ^{36}Cl (nonvolatile).

Introduction

The complexity of flow in the shallow unsaturated zone of desert soils requires the use of numerical models to evaluate flow processes and to analyze interactions and feedback mechanisms between various controlling parameters. Most numerical modeling studies focus on isothermal liquid flow and neglect the effect of vapor flow. However, vapor flow may be important, particularly near the soil surface in arid systems, where the soils are very dry and where temperature gradients are steep. Numerical models of varying complexity have been used to simulate nonisothermal liquid and vapor flow. Development of these models has been motivated by problems such as evaluation of shallow unsaturated zones, geothermal reservoirs, and nuclear waste disposal sites. This study is concerned primarily with the "weakly" nonisothermal systems of *Pruess* [1987], in which temperatures remain below the boiling point of water. Models of these weakly nonisothermal systems are generally based on the equations of *Philip and de Vries* [1957]. Application of these numerical models to evaluate subsurface water flux has been limited by lack of appropriate field data. Although field studies were conducted to evaluate the numerical model developed by *Sophocleous* [1979], test cases representing dry conditions were hypothetical because of problems with field psychro-

Paper number 93WR03252.
0043-1397/94/93WR-03252$05.00

metric measurements. Only water content data were available to evaluate results of heat and water flux simulations conducted by *Baca et al.* [1978] because temperature and water potential were not monitored.

Previous simulations of nonisothermal liquid and vapor flow in the shallow unsaturated zone of an area within the Chihuahuan Desert of Texas were restricted to 5-day periods in the summer and winter and showed that below the evaporation front, downward vapor fluxes in the summer were much greater than generally upward vapor fluxes in the winter [*Scanlon*, 1992a]. The results suggested an annual net downward vapor flux that is consistent with the observed deeper penetration of ^{3}H (volatile) relative to that of ^{36}Cl (nonvolatile).

The objective of this study was to evaluate and explain liquid and vapor fluxes in the shallow unsaturated zone of the Chihuahuan site in response to an annual climate cycle. Our approach was to use numerical simulations to interpret observed field data. In contrast to previous simulations [*Scanlon*, 1992a] that considered short-term precipitation-free periods, the full annual cycle includes alternating periods of precipitation and evaporation. The long-term monitoring record of subsurface water potentials and temperatures in this study provided initial conditions for the model and data to test model results. Because of the complexity of the system and the numerical model, there were considerable uncertainties in the soil physical properties. We made no attempt to calibrate the model, but we did use sensitivity runs to understand the physical factors that control water movement.

One major difference between this and previous studies of nonisothermal flow systems is that flow in the natural system was evaluated in this study, whereas many previous studies evaluated subsurface flow after an initial period of artificial saturation [*Hanks et al.*, 1967; *Rose*, 1968]. In addition, the 1-year period simulated is much longer than the periods (hours to days) simulated in previous studies [*Sophocleous*, 1979; *van de Griend et al.*, 1985; *de Silans et al.*, 1989]; this gives a more comprehensive view of flow processes with reduced dependence on initial conditions.

Governing Equations

Water and heat fluxes were simulated with a one-dimensional numerical code, Simulation Program for Land Surface Heat and Water Transport (SPLaSHWaTr) [*Milly*, 1982]. SPLaSHWaTr is based on the formulation of water and heat flux by *Philip and de Vries* [1957] and *de Vries* [1958], as generalized by *Milly* [1982]. Two features of SPLaSHWaTr are critical for this study and distinguish this code from many other codes that simulate nonisothermal flow in the unsaturated zone. The first is the use of matric potential rather than water content as one of the dependent variables; this allows simulation of flow in heterogeneous, variably saturated systems. The second critical feature is the specification of the upper boundary condition in terms of atmospheric forcing. Model assumptions include (1) no uptake of water by plants, (2) local hydraulic and thermal equilibrium among solid particles, air, and water, and (3) a static air phase [*Milly and Eagleson*, 1982]. The lack of water uptake by plants is appropriate for the study area because hydraulic parameters were monitored in bare soil. The assumption of local hydraulic and thermal equilibrium only breaks down at high infiltration rates in coarse soil [*Milly*, 1982]; therefore this assumption is reasonable for the study area, which is characterized by fine-grained surficial sediments. The effect of the static air phase assumption on simulation results will be discussed in a later section.

It is well-known that the relation between matric potential and water content of soils exhibits hysteresis. In this study, however, we assume that the water content is a unique function of matric potential and temperature at any time. This neglect of hysteresis is a definite limitation of this study. The SPLaSHWaTr code permits hysteresis but fails to consider the entire wetting and drying history in an internally consistent way [*Milly and Eagleson*, 1980]. We judged that it was better to neglect hysteresis altogether in this study than to use a questionable parameterization of it. Furthermore, we were not aware of any comparable model with a valid description of hysteresis, we did not have the resources to develop one, and we felt that meaningful results could be obtained without considering hysteresis. The slight hysteresis in the dependence of hydraulic conductivity on water content is also ignored here.

The SPLaSHWaTr code is fully documented by *Milly and Eagleson* [1980] and *Milly* [1982, 1984]; however, the governing equations are provided here for convenience. The governing equation for water is given by *Milly* [1982]:

$$\left[\left(1-\frac{\rho_v}{\rho_l}\right)\left.\frac{\partial\theta}{\partial\psi}\right|_T+\frac{\theta_a}{\rho_l}\left.\frac{\partial\rho_v}{\partial\psi}\right|_T\right]\frac{\partial\psi}{\partial t}+\left[\left(1-\frac{\rho_v}{\rho_l}\right)\left.\frac{\partial\theta}{\partial T}\right|_\psi+\frac{\theta_a}{\rho_l}\left.\frac{\partial\rho_v}{\partial T}\right|_\psi\right]\frac{\partial T}{\partial t}=\frac{\partial}{\partial z}\left[(K+D_{\psi v})\frac{\partial\psi}{\partial z}+(D_{Tv}+D_{Ta})\frac{\partial T}{\partial z}\right]+\frac{\partial K}{\partial z} \quad (1)$$

where ρ_v is the density of water vapor in the air-filled part of the pore space, ρ_l is the density of liquid water, θ is the volumetric liquid water content, ψ is the matric potential, θ_a is the volumetric air content, T is temperature, t is time, K is hydraulic conductivity, z is the vertical space coordinate, $D_{\psi v}$ is the isothermal vapor diffusivity, D_{Tv} is the thermal vapor diffusivity, and D_{Ta} is the transport coefficient for adsorbed liquid flow due to thermal gradients, which is ignored in this study because we believe it is negligible in comparison with D_{Tv} at the study site. $D_{\psi v}$ and D_{Tv} are given by *Milly* [1982] and *Milly and Eagleson* [1980]:

$$D_{\psi v}=\frac{D_{atm}}{\rho_l}\alpha\theta_a\left.\frac{\partial\rho_v}{\partial\psi}\right|_T=\frac{D_{atm}}{\rho_l}\alpha\theta_a\frac{g\rho_v}{RT}$$

$$D_{Tv}=\frac{D_{atm}}{\rho_l}f\zeta\left.\frac{\partial\rho_v}{\partial T}\right|_\psi=\frac{D_{atm}}{\rho_l}f\zeta\left(h\frac{\partial\rho_{vs}}{\partial T}-\frac{g\rho_v\psi}{RT^2}\right)$$

in which D_{atm} is the molecular diffusivity of water vapor in air, α is the tortuosity factor, g is the acceleration due to gravity, R is the gas constant for water vapor,

$$f=n \qquad \theta\le\theta_k$$

$$f = \theta_a + \frac{\theta_a}{n - \theta_k}\theta \qquad \theta_k < \theta$$

in which n is porosity, θ_k is the highest water content at which unsaturated hydraulic conductivity (K_u) is much lower than $D_{\psi v}$, $\zeta = (\nabla T)_a/\nabla T$, $(\nabla T)_a$ being average temperature gradient in the air phase, h is relative humidity, ρ_{vs} is saturated vapor density, and T is absolute temperature (K).

The heat equation as given by *Milly* [1982] is

$$\left(C + H_1 \left.\frac{\partial \rho_v}{\partial T}\right|_\psi + H_2 \left.\frac{\partial \theta}{\partial T}\right|_\psi\right)\frac{\partial T}{\partial t} + \left(H_1 \left.\frac{\partial \rho_v}{\partial \psi}\right|_T + H_2 \left.\frac{\partial \theta}{\partial \psi}\right|_T\right)\frac{\partial \psi}{\partial t} = \frac{\partial}{\partial z}\left[\lambda \frac{\partial T}{\partial z} + \rho_l(LD_{\psi v} + gTD_{Ta})\frac{\partial \psi}{\partial z} - c_l(T - T_0)q\right] \qquad (2)$$

where

$$H_1 = [L_0 + c_p(T - T_0)]\theta_a$$

$$H_2 = (c_l\rho_l - c_p\rho_v)(T - T_0) - \rho_l W - \rho_v L_0$$

C is the volumetric heat capacity of the soil, λ is the effective thermal conductivity, L is the latent heat of vaporization of water, c_l is the specific heat of liquid water, L_0 is the value of L at an arbitrary reference temperature T_0, q is the total water flux, c_p is the specific heat of water vapor at constant pressure, and W is the differential heat of wetting of the soil. The volumetric heat capacity of the soil is a weighted mean of the capacities of its components [*de Vries*, 1963]. The effective thermal conductivity of the soil and ζ were calculated according to *de Vries* [1963], and the differential heat of wetting was calculated according to *Groenevelt and Kay* [1974].

The effects of temperature enter directly through the temperature gradients in (1) and (2) and indirectly through the temperature dependence of the matric potential, hydraulic conductivity, and vapor diffusivity. The temperature dependence of the matric potential was calculated by introducing the variable Ψ, in essence, a temperature corrected potential, which is assumed to be a function of water content only [*Milly*, 1984]:

$$\Psi(\theta) = \psi \exp[-C_\psi(T - T_0)] \qquad (3a)$$

where

$$C_\psi = \frac{1}{\psi}\left.\frac{\partial \psi}{\partial T}\right|_\theta \qquad (3b)$$

T is temperature and T_0 is an arbitrary reference temperature. The surface tension model generally underestimates observed values of C_ψ [*Wilkinson and Klute*, 1962; *Nimmo and Miller*, 1986]. In an early application of SPLaSHWaTr, *Milly* [1984] assigned a value of -0.0068K^{-1} to C_ψ [*Milly*, 1984]; this value is approximately 3 times that predicted by the surface tension model [*Philip and de Vries*, 1957]. *Milly*'s [1984] value was retained for simulations in this study. The temperature dependence of the hydraulic conductivity (K) is given by

$$K = K_s K_r(\theta)\nu(T_0)/\nu(T) \qquad (4)$$

where K_s is the saturated hydraulic conductivity at the reference temperature T_0, K_r is the relative hydraulic conductivity (which is a function of water content [θ]), and ν is the kinematic viscosity [*Milly*, 1984]. In fact, this approach may underestimate the sensitivity of hydraulic conductivity to temperature by a factor of 2 or 3 [*Giakoumakis and Tsakiris*, 1991].

If the surface does not become saturated, then the surface boundary condition associated with the water flux is

$$(q/\rho_l)_{z=0} = P - E \qquad (5a)$$

where P is precipitation and E is evaporation [*Milly*, 1984]. The evaporation rate is defined by the aerodynamic diffusion relation [*Milly*, 1984]. When the surface becomes saturated, the boundary condition can be shown by

$$\psi|_{z=0} = 0 \qquad (5b)$$

where the depth of ponded water at the surface is negligible. In that situation, the model determines the surface influx, and any excess precipitation produces runoff. This surface boundary condition fails to allow for infiltration of runoff produced upstream of our ephemeral channel site. Such runoff events are rare and short lived. Furthermore, they would tend to occur when the model predicts surface saturation and maximum possible infiltration, in which case the additional water available from upstream could not infiltrate.

The surface boundary condition associated with the heat flux equation is [*Milly*, 1984]

$$q_h|_{z=0} = -(1 - A)I_s - \varepsilon[I_{ld} - \sigma(T|_{z=0} + 273)^4] + \rho_l[L + c_l(T|_{z=0} - T_0)]E - \rho_l c_l(T_a - T_0)]E - \rho_l c_l(T_a - T_0)P + H \qquad (6)$$

where q_h is the soil heat flux, A is albedo, I_s is the incoming solar radiation, ε is emissivity, I_{ld} is the incoming atmospheric radiation, σ is the Stefan-Boltzmann constant, T is temperature (°C), $T + 273$ is absolute temperature (K), and H is the turbulent diffusion of sensible heat into the atmosphere.

The one-dimensional forms of the governing partial differential water and heat equations are solved by the Galerkin finite element method in SPLaSHWaTr. The resulting nonlinear system of ordinary differential equations is solved by finite differencing and Picard iteration at each time step. The water and heat equations are solved alternately to maintain the tridiagonal nature of the matrix. Convergence and mass conservation problems are sometimes cited as problems in ψ based numerical models; such problems were eliminated in SPLaSHWaTr by introduction of a new numerical technique [*Milly*, 1985] and by automatic control of the time step size, allowing high accuracy to be achieved without excessive use of computing time. The code was implemented on a MicroVax computer workstation.

Numerical Simulations

Overview

We performed four 1-year (October 1989 to September 1990) simulations of water and heat fluxes in response to

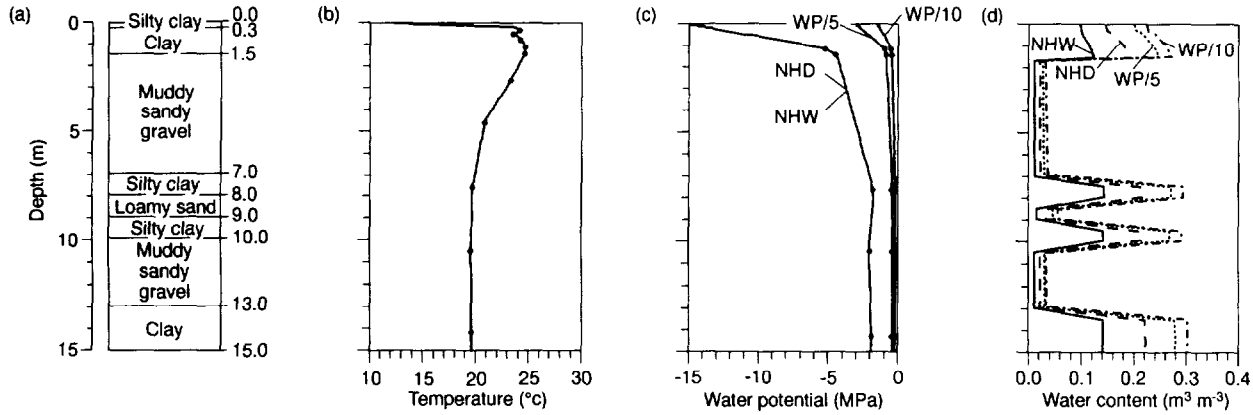

Figure 1. (a) Variations in soil texture from borehole 50S [*Scanlon*, this issue, Figure 1] with depth for simulated region. (b) Temperature and (c) water potential profiles measured by in situ psychrometers (P and 20P [*Scanlon*, this issue, Figure 1]) on October 1, 1989. These profiles constitute the initial conditions for the 1-year simulations. (d) Corresponding water content profiles for the nonhysteretic simulations were estimated from the measured water potential data using the main drying (NHD) and main wetting (NHW) curves for the materials at each depth; WP/5 and WP/10 profiles represent the water content profiles calculated with the main drying function from initial water potentials that were divided by 5 and 10.

atmospheric forcing. Hysteresis in the soil hydraulic properties was ignored in all simulations in this study. Simulation nonhysteretic drying (NHD) employed the measured main drying data to describe nonhysteretic water retention; nonhysteretic wetting (NHW) used the main wetting data estimated from the measured main drying data. The purpose of running both NHD and NHW was to obtain some insight into the sensitivity of long-time simulations to differences in water retention functions and associated differences in relative hydraulic conductivity, which was derived from the retention curve. (Comparison of NHD and NHW may also give some crude estimate of the importance of hysteresis, although such inferences would be tenuous because the computed variables in NHD and NHW do not necessarily bound the variables that would be computed with the consistent hysteretic soil.) Both NHD and NHW were initialized with field measurements of water potential and temperature. Two other simulations (WP/5 and WP/10) were identical to NHD, except that the initial values of water potential inferred from field measurements were increased by dividing initial water potentials by 5 and 10. The purpose of these additional simulations was to provide an understanding of the sensitivity of the simulation to the initial condition. Further details on initial conditions, boundary conditions, water retention, and hydraulic conductivity are provided in the remainder of this section.

Initial and Boundary Conditions

Initial conditions (Figure 1) were based on water potential and temperature monitored by in situ psychrometers that were installed in an ephemeral stream setting [*Scanlon*, this issue, Figure 1, 20P and P]. Water potentials were out of range of the in situ psychrometers in the upper 0.8 m of the soil; therefore the initial surface water potential (for NHD and NHW) was assigned a value of −15 MPa, which is approximately equal to the lowest water potential measured by the laboratory psychrometer on soil sampled from the field site. Rainfall data were mostly obtained from the R_E gauge, which is located approximately 2 km east-northeast of the psychrometers at 20P and P [*Scanlon*, this issue, Figure 1]. The R_E gauge malfunctioned in September and December 1989 and August 1990, and data for these months were obtained from the other gauges (R_W gauge September 1989; R_C gauge December 1989 and August 1990 [*Scanlon*, this issue, Figure 1]). Rainfall of 207 mm for the year simulated (October 1, 1989 to September 30, 1990) (Figure 2) was lower than the long-term (1966–1987) mean annual rainfall of 280 mm for the Fort Hancock observation station situated 18 km southwest of the study area. Rainfall occurred primarily from July through September 1990. The initial temperature at the soil surface was approximated by the soil temperature measured at a 0.01-m depth. The upper boundary conditions were based on hourly averages of air

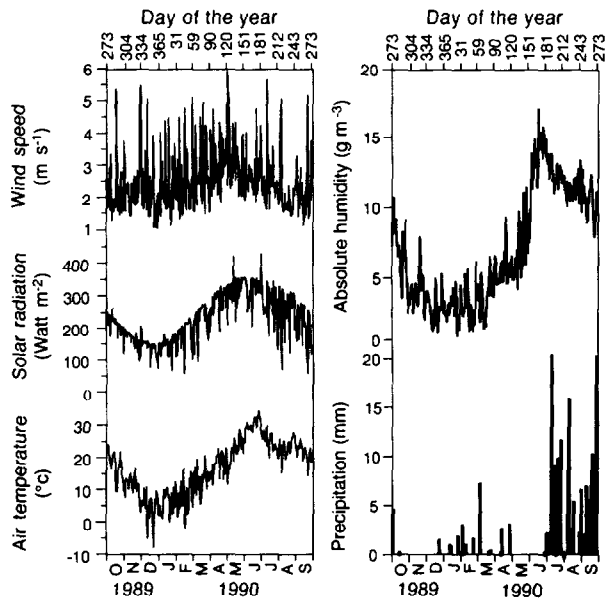

Figure 2. Daily mean wind speed, solar radiation, air temperature, absolute humidity, and daily precipitation at the study site, October 1, 1989, through September 30, 1990.

Table 1. Hydraulic Parameters for Soil Textures Used in the Simulations

Parameters	Clay	Silty Clay	Loamy Sand	Muddy Sandy Gravel
K_s, cm s^{-1}	2.70×10^{-6}	3.20×10^{-6}	3.70×10^{-3}	2.60×10^{-3}
Porosity	0.51	0.47	0.45	0.41
θ_u	0.48	0.42	0.41	0.37
a^d	−80	−50	−2	−1
a^w	−80	−50	−2	−1
b^d	−2.632	−2.067	−0.430	−0.560
b^w	−3.856	−1.808	−0.562	−0.664
c^d	0.08149	0.07875	0.00898	0.0078
c^w	0.0522	0.0526	0.0051	0.0041
θ_k^d	0.13	0.11	0.034	0.029
θ_k^w	0.12	0.11	0.021	0.019

Superscripts d and w refer to main drying and main wetting curves, respectively.

temperature, solar radiation, wind speed, and absolute humidity measured from October 1, 1989, through September 30, 1990, 2 m above the soil surface at a meteorological station approximately 1.6 km northeast of 20P and P [*Scanlon*, this issue, Figure 1]. Daily averages of these parameters were plotted to evaluate seasonal fluctuations (Figure 2). Air temperature and solar radiation were highest in the summer. Wind speed was characterized by large short-term fluctuations. The absolute humidity was highest in the summer of 1990, when rainfall and temperature were highest. Incoming long-wave radiation was calculated according to *Milly and Eagleson* [1982]. Values of albedo for dry (0.2) and wet (0.1) silt loam [*Milly and Eagleson*, 1982] were assigned to the surficial sediments. A surface roughness value of 25 mm, based on previous analyses [*Scanlon*, 1992a], was used in the simulations and is a reasonable value for bare soil.

Zero gradients of water potential and temperature were assigned as the lower boundary (15-m depth) conditions. At this depth, temperature fluctuations are known to be negligible, and water flow is assumed to be controlled by gravity. Nodal spacing ranged from 0.25 mm near the soil surface to 500 mm at depth; the 15-m section of the unsaturated zone was represented by 57 elements. Previous simulations showed that increases and decreases in grid size did not affect the output [*Scanlon*, 1992a]. The time step size was controlled automatically so that temperature would not change by more than 0.1°C or water content by more than 0.001 m^3 m^{-3} during a time step.

Hydraulic Parameter Estimation Methods

Soil textures for the model domain were based on grain-size analyses of soil samples from borehole 50 [*Scanlon*, this issue, Figure 1]. Material properties were assigned to these soil textures on the basis of laboratory retention data for soils of similar texture that ranged from clay to muddy sandy gravel (Figure 1, Table 1). Experimental data on soil water desorption were fitted to determine a main drying curve, $\theta_d(\Psi)$, described by the following function [*Brooks and Corey*, 1964; *Milly and Eagleson*, 1982] (Figure 3, Table 1):

$$\theta_d(\Psi) = \min \{\theta_u,\ \theta_u[(\Psi/a)^b - (-10^5/a)^b] + c[5 - \log(-\Psi)]\} \quad (7)$$

where Ψ is in meters, θ_u is the water content obtained upon rewetting and is taken to be 90–95% of the porosity following *Mualem* [1974] because of air entrapment, and a, b, and c are fitting parameters. This water retention function was employed to describe nonhysteretic soil water retention in the NHD simulation. For the NHW simulation, the main wetting curve $\theta_w(\Psi)$ was used instead. The main wetting curve was estimated from the measured main drying data by the independent domain theory [*Mualem*, 1977]:

$$\theta_d(\Psi) = [2 - \theta_u^{-1}\theta_w(\Psi)]\theta_w(\Psi) \quad (8)$$

Data on saturated hydraulic conductivity were obtained from field and laboratory measurements (Table 1) as described by *Scanlon* [this issue]. The unsaturated hydraulic conductivity (Figure 4) was calculated by numerical integration of the following equation [*Mualem*, 1976]:

$$K_u(\theta) = \left(\sqrt{S_e}\left[\int_0^{S_e} \frac{dS}{\Psi(S)}\right]^2 \left[\int_0^1 \frac{dS}{\Psi(S)}\right]^{-2}\right) K_s \quad (9)$$

where S_e is the effective saturation:

$$S_e = \frac{\theta - \theta_k}{\theta_u - \theta_k}$$

θ_k is the value of water content at which liquid flow becomes negligible (specified as the water content at which isothermal vapor diffusivity is an order of magnitude greater than

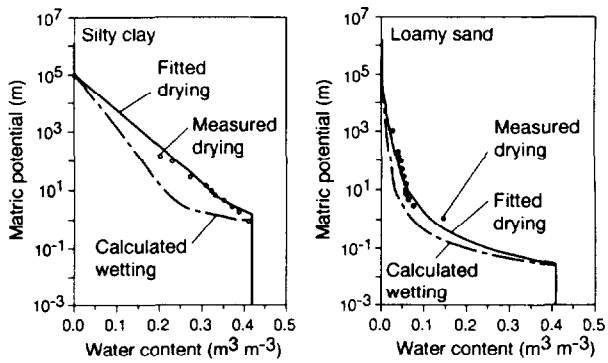

Figure 3. Measured main drying water retention data; fitted analytic function [*Brooks and Corey*, 1964; *Milly and Eagleson*, 1982] and estimated main wetting function [*Mualem*, 1977; *Brooks and Corey*, 1964; *Milly and Eagleson*, 1982].

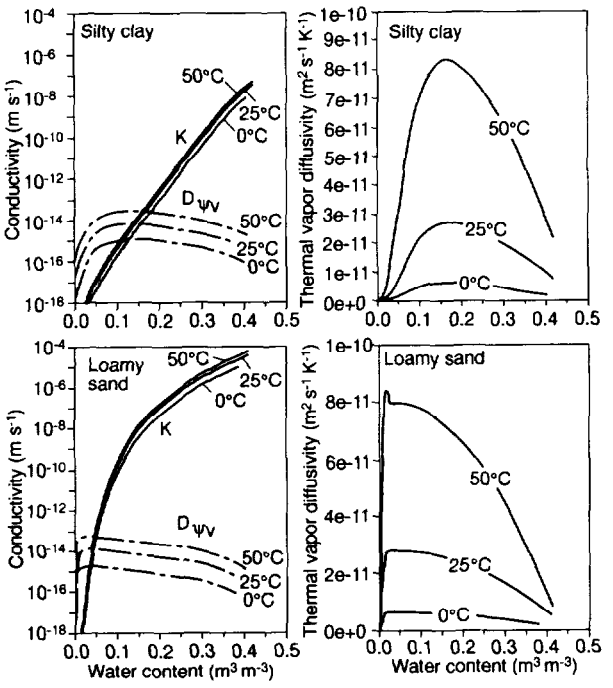

Figure 4. Liquid hydraulic conductivity (K) and isothermal ($D_{\psi v}$) and thermal (D_{Tv}) vapor diffusivity as a function of water content and temperature for representative soil textures.

unsaturated hydraulic conductivity [*Milly and Eagleson*, 1982]), and S is a dummy integration variable for S_e.

The percent quartz, other minerals, and organic matter were input for soil thermal conductivity, which was calculated according to the method of *de Vries* [1963] [*Milly*, 1984]. Isothermal and thermal vapor diffusivities were calculated according to *Milly* [1982] and *Milly and Eagleson* [1980]. The temperature and water content dependencies of liquid hydraulic conductivity and of isothermal and thermal vapor diffusivities for representative soil textures are shown in Figure 4.

Results and Discussion

Comparison of NHD Simulation With Measurements

There is remarkable consistency between the NHD-simulated water potentials and the available field measurements. Figure 5 shows simulated and measured water potentials at 0900 hours for the 1-year period at depths of 0.3, 0.5, 0.8, 1.1, 1.4, and 10.5 m. Computed water potentials at the 10.5-m depth were temporally invariant and were similar to measured water potentials at that depth. At depths of 1.4 and 1.1 m, the measured and simulated seasonal changes in water potentials were very similar; however, the simulated values were somewhat higher than the measured values throughout the 1-year period and had somewhat smaller seasonal variations. Water potentials at 0.3, 0.5, and 0.8 m depths were below the measurement range of the in situ psychrometers (<-7 to -8 MPa) for most of the monitoring period; computed water potentials were also less than -8 MPa. Measured water potentials increased to ≥ -7 MPa at the 0.3-m depth in September 1990 after summer rain, and this change in water potentials was reproduced by the simulation.

The NHD simulation of seasonal changes of temperature at 0900 hours is also in good agreement with the field

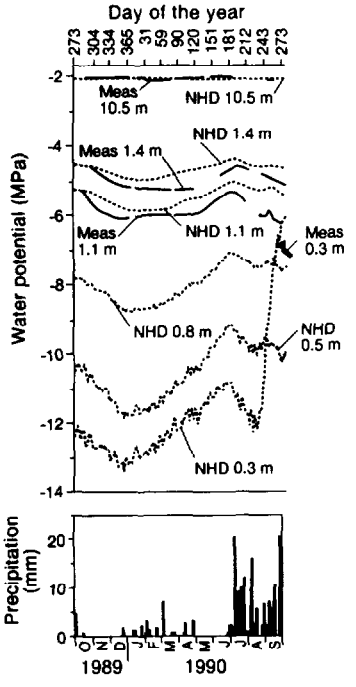

Figure 5. Time evolution of daily (0900 hours) measured and computed (NHD) water potentials and daily precipitation for the 1-year simulation period.

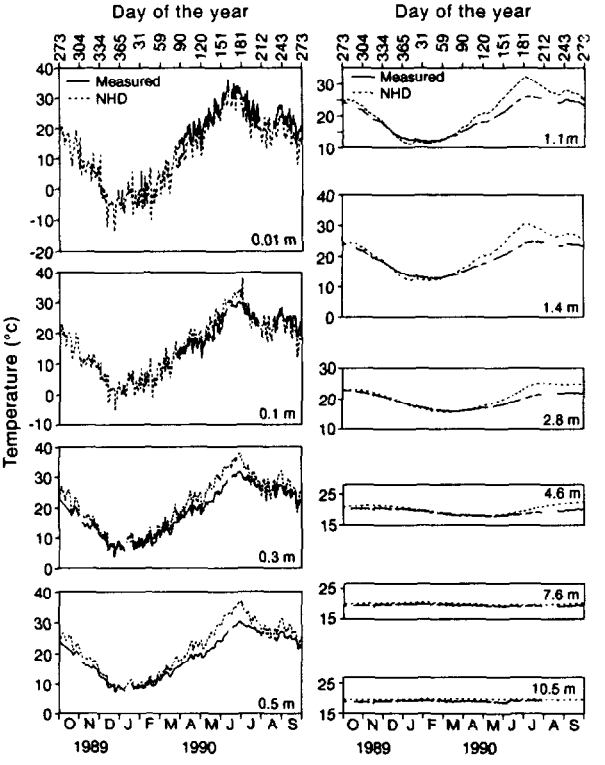

Figure 6. Time evolution of daily (0900 hours) measured and computed (NHD) temperatures for the 1-year simulation period.

measurements (Figure 6). Measured and simulated values both show the well-known extinction and phase shift of the annual surface temperature wave with depth. There is a positive error in simulated peak temperatures at depths of 0.3 m and below, despite a relatively accurate simulation of the temperature at 0.01- and 0.1-m depths. This can be attributed to errors in the prescribed (and uncalibrated) thermal properties of the soil.

The similarity between Figures 5 and 6 suggests an explanation for the measured depth and time dependencies of water potential and their faithful reproduction in the simulation, which was achieved despite gross uncertainties in hydraulic properties. Ignoring the effect of the surface water input in the summer of 1990, we can see that the attenuation and phase shift of water potentials with depth are similar to those of temperature. We propose that the water potential changes are driven primarily by the temperature changes, with water content remaining relatively constant, according to (3a). For the model simulation, this hypothesis is confirmed by Figures 7a and 7b, which compare modeled potentials at depths of 1.1 and 1.4 m with those computed from (3a) using the modeled soil temperatures and the initial values of Ψ. Figures 7c and 7d compare the potentials computed from (3a), using field-measured temperatures and $C_\psi = -0.0068$ K^{-1}, with the field-measured water potentials. The computed potentials change considerably less than the measured values. However, it should be kept in mind that the true value of C_ψ is quite uncertain, and may vary with depth and time. A value of $C_\psi = -0.015$ K^{-1} provides much better, but still far from perfect, agreement between water potentials computed using (3a) and field measurements except after June 1990. Thus the field data are generally consistent with the proposed hypothesis if one accepts an average field-inferred value for C_ψ of approximately -0.015 K^{-1}.

Consistent with the time and depth behaviors of water potential noted above, the changes in water storage associated with individual rainfall events were confined mainly to the top 0.3 m of soil. Water potential data for this upper layer are unavailable for comparison with simulated results. Simulated water potentials in this zone ranged from 0 to −387 MPa. The dominant effect of rainfall in the summer of 1990 is shown by substantial increases in computed water potentials and water content at this time (Figures 8 and 9).

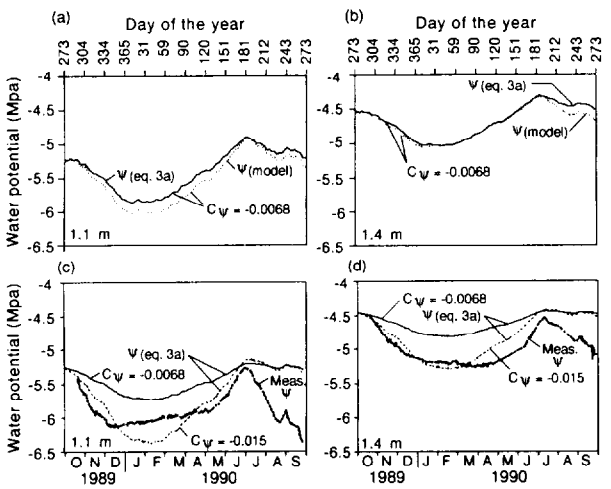

Figure 7. Comparison of modeled water potentials at (a) 1.1- and (b) 1.4-m depths with those computed from (3a) using the modeled soil temperatures and initial values of Ψ. Comparison of field-measured water potentials at (c) 1.1- and (d) 1.4-m depths with those computed from (3a) using field measured temperatures and values of $C_\psi = -0.0068°K^{-1}$ and $C_\psi = -0.015°K^{-1}$.

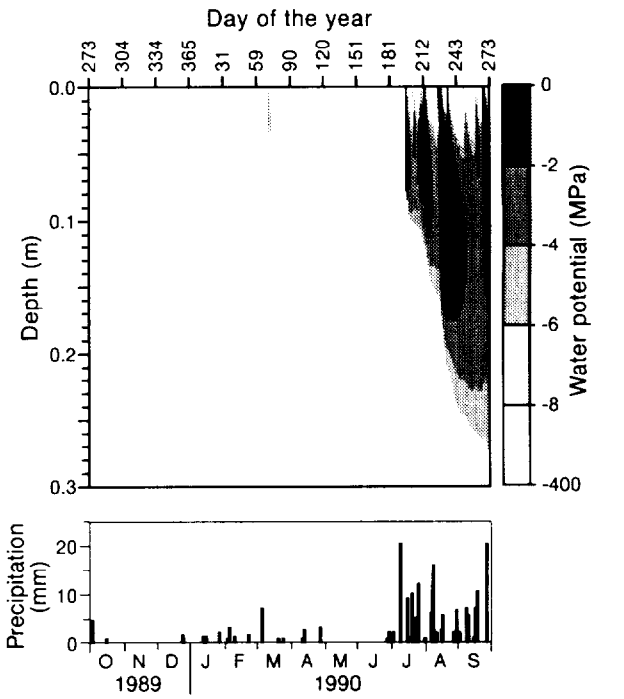

Figure 8. Time evolution of computed water potentials based on daily 0900 hours output from NHD and daily precipitation. Water potential output from the simulation was for 20 depths that range from 0.0025 m near the surface to 0.2-m intervals at depth; water potentials in between these levels were interpolated linearly and are shown on a linear scale as gray tones.

Another important feature of the measurements, which is present also in the simulation, is the vertical gradient in water potential. The measured annual mean water potential decreased from −2.1 MPa at 10.5 m depth to −4.7 MPa at 1.4 m depth and −5.4 MPa at 1.1 m depth; this indicates a driving force for upward liquid water flow. Reproduction of this gradient in the simulation could be attributed to its specification in the initial condition; such a possibility cannot be eliminated without knowing how long the effective "memory" of the system is. This issue is discussed in the next section.

The water balance computed for the simulated year is summarized in Table 2; the accumulation of this balance over time is shown in Figure 10. A total precipitation of 207 mm was balanced by a 162-mm evaporative loss to the atmosphere, 10-mm surface runoff due to surface saturation during storms, and an increase of storage in the modeled soil (0–15 m depth) of 35 mm. The efflux from the bottom of the modeled soil was negligible. Measurements of evaporation are not available for comparison. Analysis of stream gauge data for the site suggests that 0.2–2% of precipitation runs off (S. Akhter, personal communication, 1990), which would result in a 0.4- to 4-mm runoff for the simulated year. These values are slightly lower than the simulated runoff of 10 mm.

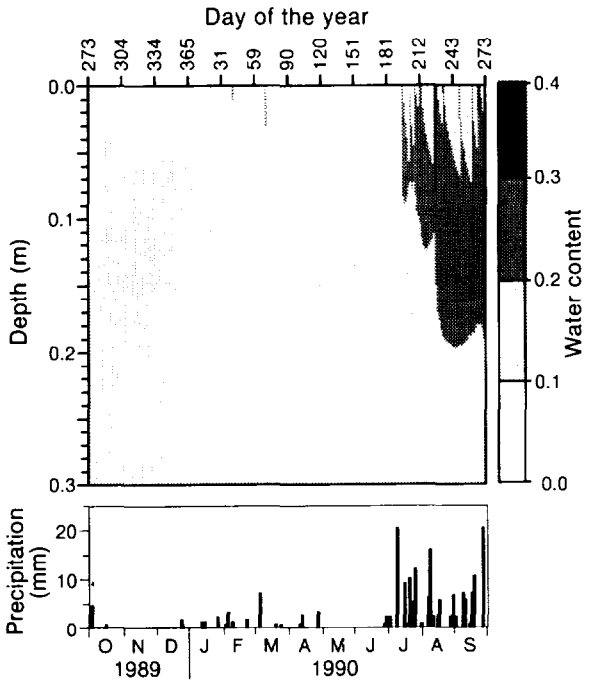

Figure 9. Time evolution of computed water contents based on daily 0900 hours output from NHD and daily precipitation. See Figure 8.

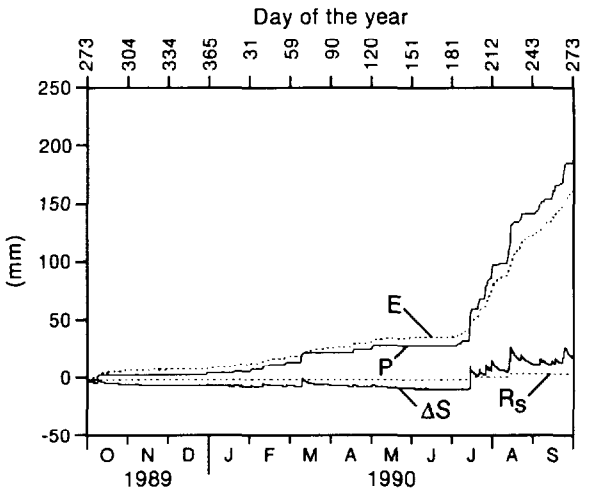

Figure 10. Measured cumulative precipitation (P), computed cumulative evaporation (E), surface runoff (R_s), and storage change (ΔS) for NHD.

Rainfall in summer was approximately 7 times higher than that in winter and resulted in high surface runoff, evaporation, and storage change in the summer.

Mechanisms of Water Transport in the Model

In this section, we discuss the simulation results in terms of the various fluxes. Vertical fluxes of water can be decomposed into fluxes of liquid ($-K\partial\psi/\partial z$), which are driven by water potential gradients, and diffusive fluxes of vapor, which are driven by vapor pressure gradients that are in turn caused by water potential gradients (isothermal vapor flux, ($-D_{\psi v}\partial\psi/\partial z$)) and temperature gradients (thermal vapor flux ($-D_{Tv}\partial T/\partial z$)). The sign conventions for subsurface fluxes is that upward fluxes are positive and downward fluxes are negative.

In the upper 0.3 m of the soil, the direction, magnitude, and mechanism of water fluxes vary in response to the intermittent wetting and drying by weather events discussed earlier. As a consequence, it is not easy to characterize them succinctly. A detailed analysis of water fluxes in this near-surface layer revealed that the dominant process for downward water movement was liquid flow (Figure 11a). Very close to the surface, upward isothermal vapor fluxes were significant. The annual evaporation of 162 mm may be compared to mean annual isothermal vapor fluxes of 128, 86, 35, and 16 mm at depths of 1.25, 7.5, 25, and 55 mm. Cumulative downward liquid flux in summer penetrated to a much greater depth (0.3 m) than downward liquid flux in winter (0.05 m) because of high summer rain (Figure 12).

Below the 0.3-m depth, water fluxes varied relatively little. The dominant term was the thermal vapor flux, which varied with season and depth following the temperature gradient. In the annual mean, its downward values in summer outweighed the upward values in winter (Figure 12), giving cumulative annual downward thermal vapor fluxes of 1.5, 0.9, 0.65, and 0.17 mm yr^{-1} at depths of 0.5, 1.0, 2.0, and 5.0 m (Figure 11). Thermal vapor flux was essentially unbalanced by the other water fluxes in the simulation. As a

Table 2. Soil Water Balance

	P, mm	E, mm	R_s, mm	ΔS, mm	Deep Drainage, mm
NHD Oct. 1, 1989, to Sept. 30, 1990	207	162	9.9	35.2	-4.8×10^{-3}
NHD June 21, 1990, to Sept. 21, 1990	138	109	5.5	23.3	-1.2×10^{-3}
NHD Dec. 21, 1989, to March 21, 1990	19	17	0.00	1.6	-1.2×10^{-3}
NHW Oct. 1, 1989, to Sept. 30, 1990	207	156	19.3	32.1	-1.8×10^{-4}
NHW June 21, 1990, to Sept. 21, 1990	138	105	12.3	20.0	-4.5×10^{-5}
NHW Dec. 21, 1989, to March, 21, 1990	19	17	0.0	2.0	-7.9×10^{-4}
WP/5 Oct. 1, 1989, to Sept. 30, 1990	207	174	10.2	22.9	-1.3×10^{-1}
WP/10 Oct. 1, 1989, to Sept. 30, 1990	207	182	10.4	14.8	-5.5×10^{-1}

P, precipitation; E, evaporation; R_s, surface runoff; ΔS, storage change; NHD and NHW, nonhysteretic drying and wetting simulations, respectively. WP/5 and WP/10 are similar to NHD except that the initial water potentials have been increased.

result, there was a net convergence of total water flux and hence an accumulation of water at all depths below the near surface layer. The associated rate of change of water content was 0.0018, 0.0003, 0.0003, and 0.0001 $m^3\ m^{-3}\ yr^{-1}$ at depths of 0.5, 1.0, 2.0, and 5.0 m, respectively. The low water flux throughout most of the domain confirms the earlier suggestion that the preservation of the initial water potential distribution was a major factor in the simulation.

Possible Causes of Lack of Equilibrium in the Model

We have shown that simulated thermal vapor flux convergence in NHD was unbalanced by other water fluxes below 0.3 m. It is important to consider whether such a situation is likely to occur in the field. On the basis of sensitivity simulations and approximate calculations, it appears that the sign and magnitude of the net annual convergence of thermally driven vapor flux are realistic, robust, and persistent through the years, as long as the soil below 0.3 m does not become so desiccated (potential of approximately -10^4 m (−100 MPa) or lower) that the relative humidity of soil air drops far below saturation. Furthermore, the isothermal vapor flux appears to be too small to balance the thermal vapor flux. This implies that there is an annual mean source of liquid water below 0.3 m (and a related sink near the surface) which must be balanced by some combination of changes in liquid storage and divergences of liquid flux.

In the short term, annual storage changes could balance vapor convergence below 0.3 m, but in the long term liquid flux divergence would have to occur. In our simulation, values of hydraulic conductivity were far too small for such liquid flow compensation to occur, and storage changes resulted instead. If the same forcing had been continued through many annual cycles, the soil would have eventually moistened to the point where the source term was balanced in the annual mean, by liquid efflux, either upward or downward, from the source region.

The question naturally arises as to whether the source was balanced by storage change or liquid flux divergence in the field during the year that we simulated. If hydraulic conductivity values were actually greater than those computed from (9), then a return flow of liquid toward the surface, driven by the observed hydraulic gradient, could have balanced the thermal vapor flux. Indeed, the necessary increase in conductivity values would be within the known range of errors of equations such as (9). The compensating upward liquid return flow would imply in situ values of hydraulic conductivity on the order of 3.4×10^{-14}, 6.0×10^{-13}, and 3.0×10^{-13} m s^{-1} at depths of 1, 2, and 3 m. The alternative hypothesis is that the liquid fluxes were, indeed, negligible in the field, and that storage increases occurred instead, as in the model. Such behavior might be expected if the year under consideration were somehow anomalous relative to the preceding years; if prolonged drying of the soil below 0.3 m had occurred in recent history, then the model-inferred positive trend in water content could represent a recovery from the dry period. There are insufficient data available to determine whether the net downward thermal vapor flux was balanced by storage change or liquid flux in the field.

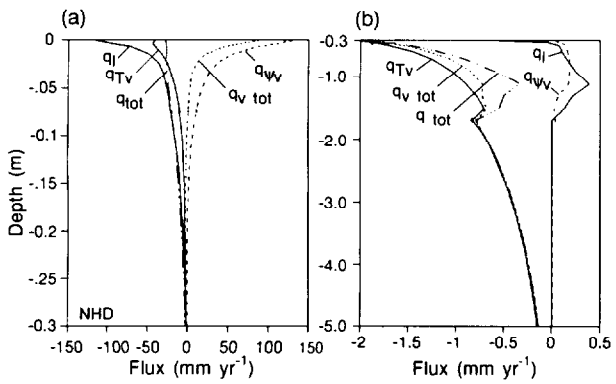

Figure 11. Variations in annual cumulative liquid (q_l), isothermal vapor ($q_{\psi v}$), thermal vapor (q_{Tv}), total vapor ($q_{v\ tot}$), and total (liquid plus vapor, q_{tot}) flux for (a) the upper 0.3 m and (b) for 0.3–5 m for NHD.

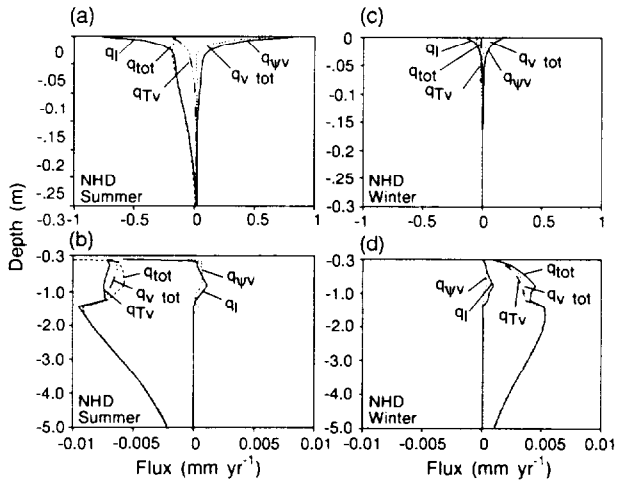

Figure 12. Variations in liquid (q_l), isothermal vapor ($q_{\psi v}$), thermal vapor (q_{Tv}), total vapor ($q_{v\ tot}$), and total (liquid plus vapor, q_{tot}) flux for (a) the upper 0.3 m and (b) 0.3–0.5 m in summer (June 21 to September 21), and (c) the upper 0.3 m and (d) 0.3–5 m in winter (December 21 to March 21) for NHD.

Model Sensitivity to Water Retention Function

Simulations NHD and NHW used the same initial profiles of water potential and temperature. However, initial water contents were much lower in NHW than in NHD because soil holds less water at a given potential when it is wetting than when it is drying (Figure 1). Differences between main wetting and drying curves at the prevailing water potentials were greater for fine-textured soils than for coarse-textured soils (Figure 3). Thermal properties of the soils were minimally affected by the difference in initial soil water content. At depths greater than 0.3 m, the agreement between measured and simulated water potentials and temperatures found in NHD was present also in NHW. This insensitivity to soil hydraulic properties, within the range considered here, is consistent with our hypothesis that the measured and simulated water potential fluctuations below the near-surface zone are controlled primarily by temperature variations. However, it should be kept in mind that these results were obtained in a model whose hydraulic conductivity, we have argued, may be too low.

The annual water balance for NHW is given in Table 2;

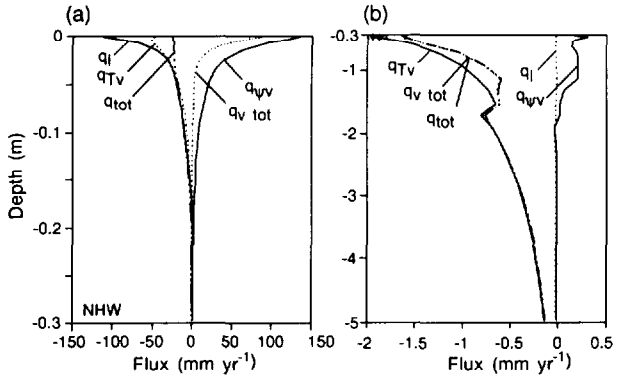

Figure 13. Variations in annual cumulative liquid (q_l), isothermal vapor ($q_{\psi v}$), thermal vapor (q_{Tv}), total vapor ($q_{v\ tot}$), and total (liquid plus vapor, q_{tot}) flux for (a) the upper 0.3 m and for (b) 0.3–5 m for NHW.

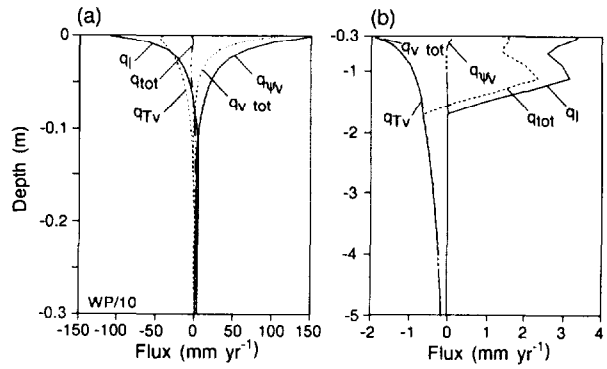

Figure 15. Variations in annual cumulative liquid (q_l), isothermal vapor ($q_{\psi v}$), thermal vapor (q_{Tv}), total vapor ($q_{v\ tot}$), and total (liquid plus vapor, q_{tot}) flux for (a) the upper 0.3 m and for (b) 0.3–5 m (b) for WP/10.

differences between NHD and NHW are relatively small. The difference in hydraulic properties apparently changes the ability of the soil to absorb the heaviest rainfalls, with decreased infiltration occurring in the NHW case. This loss of input is compensated by reductions in water accumulation and evaporation relative to those in NHD. The relative magnitudes of cumulative liquid and vapor fluxes in the near-surface layer in NHW (Figure 13) were similar to those in NHD (Figure 11).

The uncompensated thermal vapor flux convergences below the 0.5-m depth found in NHD were present also in NHW (Figures 11 and 13). Magnitudes of thermal vapor fluxes were nearly the same for NHD and NHW; mean annual values differed by less than 10% at most depths. Because of the lower water contents in NHW, the hydraulic conductivities and associated upward liquid fluxes below the 0.3-m depth were even smaller in NHW than in NHD. Liquid fluxes were typically reduced by factors of 10 in the coarse-grained sediments and by factors of 30 in the fine-grained sediments. The NHW simulation thus confirmed that the deeper liquid fluxes are highly sensitive to the assumed hydraulic properties. This is a consequence of the fact that the profile of water potential remains almost frozen at its initial shape for the entire simulation.

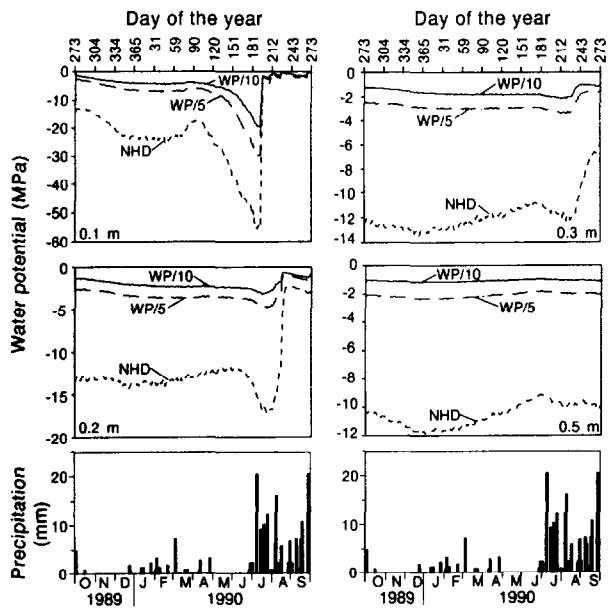

Figure 14. Time evolution of water potentials for NHD, WP/5, and WP/10 for selected depths and daily precipitation.

Model Sensitivity to Initial Water Potentials

In simulations WP/5 and WP/10, only the initial conditions differ from NHD. Differences in initial water potential among NHD (−15 to −2 MPa), WP/5 (−3 to −0.4 MPa), and WP/10 (−1.5 to −0.2 MPa) are much greater than the standard error associated with psychrometer calibration (±0.2 MPa). Because the three simulations differed only in their initial water potentials, simulations for these three cases would be expected to converge to the same solution at sufficiently large time. Water potentials for the three simulations yielded identical solutions in the upper 0.2 m after infiltration of summer rain (Figure 14). At depths greater than 0.2 m, the relaxation time greatly exceeded 1 year, and the higher initial water potentials in WP/5 and WP/10 were preserved through the simulation.

The water balances for WP/5 and WP/10 are given in Table 2. Because the water balance is determined mainly by the upper soil layers, and because NHD, WP/5, and WP/10 converge within 1 year in these upper layers, the difference in 1-year water balances is mainly attributable to the difference in initial storage of water in the soil and is insensitive to increased hydraulic conductivities associated with increased initial water potentials. WP/10, with the highest initial storage, experiences the smallest storage increase. The difference in storage changes of about 20 mm between NHD and WP/10 is approximately equal to the initial difference in storage within the top 0.3 m silty clay.

In the layers below 0.2 m, the effect of higher initial water potentials is opposite in sign, but otherwise similar, to the effect of changing from NHD to NHW. From about 0.2 to 2 m, the hydraulic conductivities are large enough in WP/10 to make computed upward liquid fluxes comparable to net downward thermal vapor fluxes on an annual basis (Figure 15). The sensitivity of fluxes to variations in initial water potential suggests that accurate information on initial water potentials is important, particularly below the shallow subsurface active zone. These results differ from those of isothermal liquid flow

simulations using the computer code TRACR3D [*Scanlon*, 1992b; *Scanlon et al.*, 1991]. Isothermal liquid fluxes in these simulations were insensitive to variations in initial water potentials except at very high values (>-0.1 MPa).

Comparison With Chemical Tracer Data

Chloride is nonvolatile and is restricted to liquid phase flow, whereas tritiated water is volatile and can move in both liquid and vapor phases. The $^{36}Cl/Cl$ peak was measured at a depth of 0.5 m and suggested a liquid flux of 1.4 mm yr^{-1} based on a 35-year period since peak fallout and an average water content of 0.1 m^3 m^{-3} in the top 0.5 m of the unsaturated zone [*Scanlon*, 1992a]. The ^3H profile was multipeaked and the peak at the 1.4-m depth was assumed to represent the 1963–1964 bomb pulse. The resultant water (liquid plus vapor) flux was 7 mm yr^{-1} based on a 25-year period since peak fallout and an average water content in the upper 1.4 m of 0.13 m^3 m^{-3}. The relative distribution of the two tracers suggests a vapor flux of 5.6 mm yr^{-1}. The previous 5-day summer and winter simulations suggested an annual net downward vapor flux that was consistent with the chemical tracer data [*Scanlon*, 1992a]. Because of the limited time of the simulations (5 days), the magnitude of the simulated fluxes was not compared with that suggested by the chemical tracers. The 1-year simulation in this study also suggests cumulative downward vapor flux except in the upper 0.08 m. The average value of downward vapor flux (NHD 1.1 mm yr^{-1}; NHW 0.9 mm yr^{-1}) from the 0.08- to 1.4-m depth (the depth of the ^3H peak) is the same order of magnitude as the 5.6 mm yr^{-1} vapor flux estimated from the relative distribution of the ^3H and $^{36}Cl/Cl$ tracers.

The vapor fluxes estimated from the tracer data and from the model differ by a factor of 5 or 6. If the flow system is not in equilibrium, then the simulated year could be unrepresentative of the period since bomb fallout began. However, it would seem to be very difficult to explain the noted discrepancy in terms of any interannual variability of the factors driving vapor flux, at least within the diffusion theory applied here. As was already mentioned, the thermal vapor flux calculations appear to be relatively robust. An alternative explanation is that the apparent vapor transport inferred from the tracer data is attributable to the strong seasonality of the thermal vapor flux. Seasonal thermal vapor fluxes are much larger than the annual means, yet this factor was not considered in the simple steady advection estimates of vapor flux from the tracer data. Further evaluation of this issue would be facilitated by the use of a transport model having seasonally varying liquid and vapor flux profiles.

Sources of Uncertainty

One of the greatest sources of uncertainty in these simulations is the estimated hydraulic conductivity function ($K(\theta)$). The $K(\theta)$ function is much more nonlinear than the $D_{\psi v}(\theta)$ or the $D_{Tv}(\theta)$ functions (Figure 4). Because the $K(\theta)$ function is estimated from the water retention function and saturated hydraulic conductivity (K_s), inaccuracies in the $K(\theta)$ function result from inaccuracies in the water retention functions, the K_s data, and especially in the estimation procedure. *Luckner et al.* [1989] discuss many possible sources of error in K_s measurements and suggest that the unsaturated hydraulic conductivity at a water content slightly less than saturation be used as a matching point rather than K_s. Uncertainties in the $K(\theta)$ function make it difficult to assess the relative importance of liquid and vapor transport in arid systems. Some ongoing studies are examining different procedures to obtain direct measurements of the $K(\theta)$ function (J. Hopmans, personal communication, 1992); [*Hudson*, 1992]. These laboratory measurements should provide data to evaluate various $K(\theta)$ estimation procedures. If the hypothesis advanced herein concerning balance of upward liquid and downward thermal vapor fluxes is correct, then it may be possible to estimate in situ hydraulic conductivity values from measurements of water potentials in the field in arid environments.

Simulations in this study demonstrate that most of the variations in hydraulic parameters and fluxes were found in the top 0.3 m; however, instrumentation has not been developed to monitor water potential variations in this zone. In situ thermocouple psychrometers do not work well in these shallow sediments because of steep temperature gradients. The lack of detailed measurements of water potential in the upper 0.3 m makes it impossible to evaluate the simulation results in this zone.

The conceptual model used for this study neglected hysteresis in the water retention functions. Although main wetting and main drying water retention curves bound hysteretic scanning curves, simulated liquid fluxes based on main curves do not necessarily bracket those based on hysteretic curves. There are many problems with simulating water retention hysteresis. Different procedures to estimate the main wetting function from the main drying function [*Mualem*, 1977; *Kool and Parker*, 1987] result in substantial differences in the estimated main wetting functions; this indicates that the main wetting and drying functions should be based on measured data. Even if measurements and an accurate model of water retention hysteresis are available, the saturation history of the profile must be determined, such as whether the system is initially drying or wetting, or whether sections of the profile are drying or wetting before the natural system can be simulated. The present analysis suggests that this is a serious concern, at least in principle, for the deeper soil horizons in an arid setting.

One of the assumptions in this study is that the air phase is static; however, in the unsaturated zone, the air phase is generally not static and the ability of the air phase to remain close to atmospheric pressure is attributed to the air phase being much more mobile than the water phase [*Hillel*, 1980]. Air pressure may affect both liquid and vapor fluxes. The effect on liquid flux should be negligible because air pressure gradients are small relative to water potential gradients, and air permeabilities should be sufficiently high to allow, without much pressure buildup, the needed air displacement with the computed water fluxes from the simulations. Air movement may also result in water movement in the vapor phase. Our model assumed that vapor phase transport simply results from diffusion relative to a static air phase. In fact, the air moves both as a result of displacement by a dynamic liquid phase and, more importantly, as a result of atmospheric pressure fluctuations, from wind gusts to synoptic-scale weather systems. The net effect is to increase the effective diffusion coefficient in the upper layers by a pumping action; that is, the air is breathed in and out. The effect of a separate air phase is thought to be greatest during individual storm events and should be relatively minor over the long time considered in these simulations.

Conclusions

Good agreement was found between NHD (nonhysteretic drying water retention function)–simulated and field-measured water potentials and temperatures. Below 0.3 m, attenuation and phase shift of water potentials and temperatures were similar and suggest that water potential variations may be controlled by temperature fluctuations, with little influence from changes of water content. Water balance data indicated that of the 207 mm of precipitation, 162 mm was evaporation, 10 mm was runoff, and 25 mm was increased soil water storage. Simulated surface runoff values (10 mm) were slightly higher than estimated values (0.4–4 mm) based on stream gauge data. Rainfall was much higher in summer than in winter, and summer infiltration dominated annual cumulative subsurface fluxes in the upper 0.3 m. Below this zone, downward thermal vapor fluxes were dominant and were not balanced by other fluxes. This annual cumulative downward water flux indicates that the model is not in equilibrium with its atmospheric forcing. This could indicate true disequilibrium in the field, or it may be attributable to inaccuracies in hydraulic conductivities, which may underestimate upward liquid fluxes.

Sensitivity of model results to use of the nonhysteretic wetting water retention function was examined in the NHW simulation. Use of the main wetting data resulted in much lower initial saturation distribution relative to that in NHD. Thermal properties of soil were negligibly affected by differences in initial water content. Computed water potentials and temperatures based on NHD and NHW were similar below 0.3 m, which supports the explanation that water potential variations are controlled by temperature fluctuations. Increased surface runoff in NHW relative to that in NHD was compensated by reduced water accumulation and evaporation in NHW. Below 0.3 m, smaller upward liquid fluxes in NHW relative to those in NHD suggest that liquid fluxes in this zone are sensitive to the water retention functions that enter the calculations of hydraulic conductivity.

Simulations WP/5 and WP/10 differed from NHD in that the initial water potentials were increased by dividing by 5 and 10. Water potentials in the upper 0.2 m in all three simulations converged after infiltration of summer rain; however, initial water potentials at greater depths were preserved throughout the year. Below 0.2 m, the initial water distribution remains almost unchanged for 1 year, and the increased upward liquid fluxes associated with increased initial water potential are attributed to increased unsaturated hydraulic conductivity. The water balance is determined mainly in the shallow subsurface ($\leq$0.3 m). Differences in water balance among the three simulations can be explained by variations in initial soil water storage and are negligibly affected by differences in unsaturated hydraulic conductivity associated with variations in initial water potential.

Comparison of numerical model results with chemical tracer data shows that simulated downward vapor flux below the evaporation front (0.08 m) based on these numerical simulations agrees with the deeper penetration of bomb ^{3}H (volatile) relative to that of bomb ^{36}Cl (nonvolatile). The simulated average downward vapor flux from the 0.08- to 1.4-m depth (NHD 1.1 mm yr^{-1}; NHW 0.9 mm yr^{-1}) is within the same order of magnitude as that based on the relative distribution of ^{3}H and $^{36}Cl/Cl$ (5.6 mm yr^{-1}).

This simulation research provides a greater understanding of unsaturated zone processes in desert soils. Agreement between computed and measured parameters are attributed to the robustness of the thermal calculations. These simulations also indicate some of the main sources of uncertainty, particularly in the estimated hydraulic conductivities.

Acknowledgments. This project was funded by the Texas Low-Level Radioactive Waste Disposal Authority under contract IAC (88-89) 0932. Publication of this manuscript was authorized by the Director, Bureau of Economic Geology, The University of Texas at Austin. Data processing was conducted by Y.-C. Chang, J. Liao and S. Ramachandra. A. J. Avakian, J. E. Constantz, A. Fryar, and R. W. Healy provided very helpful reviews. The manuscript was edited by B. S. Duncan. Drafting was by J. L. Lardon and S. Krepps under the direction of R. L. Dillon.

References

Baca, R. G., I. P. King, and W. R. Norton, Finite element models for simultaneous heat and moisture transport in unsaturated soils, in *Finite Elements in Water Resources*, edited by C. A. Brebbia, W. G. Gray, and G. F. Pinder, pp. 1.19–1.35, Pentech, London, 1978.

Brooks, R. H., and A. T. Corey, Hydraulic properties of porous media, *Hydrol. Pap., 3*, 27 pp., Colorado State Univ., Fort Collins, 1964.

de Silans, A. P., L. Bruckler, J. L. Thony, and M. Vauclin, Numerical modeling of coupled heat and water flows during drying in a stratified bare soil-comparison with field observations, *J. Hydrol., 105*, 109–138, 1989.

de Vries, D. A., Simultaneous transfer of heat and moisture in porous media, *Eos Trans. AGU, 39*, 909–916, 1958.

de Vries, D. A., Thermal properties of soils, in *Physics of Plant Environment*, edited by W. R. van Wijk, North-Holland, New York, 1963.

Giakoumakis, S. G., and G. P. Tsakiris, Eliminating the effect of temperature from unsaturated soil hydraulic functions, *J. Hydrol., 129*, 109–125, 1991.

Groenevelt, P. H., and B. D. Kay, On the interaction of water and heat transport in frozen and unfrozen soils, II, The liquid phase, *Soil Sci. Soc. Am. Proc., 38*, 400–404, 1974.

Hanks, R. J., H. R. Gardner, and M. L. Fairbourn, Evaporation of water from soils as influenced by drying with wind or radiation, *Soil Sci. Soc. Am. Proc., 31*, 593–598, 1967.

Hillel, D., *Fundamentals of Soil Physics*, 413 pp., Academic, San Diego, Calif., 1980.

Hudson, D. B., A transient method for estimating the hydraulic properties of dry unsaturated soil cores, Ph.D. dissertation, 294 pp., N. M. State Univ., Las Cruces, 1992.

Kool, J. B., and J. C. Parker, Development and evaluation of closed-form expressions for hysteretic soil hydraulic properties, *Water Resour. Res., 23*, 105–114, 1987.

Luckner, L., M. T. van Genuchten, and D. R. Nielsen, A consistent set of parametric models for the two-phase flow of immiscible fluids in the subsurface, *Water Resour. Res., 25*, 2187–2193, 1989.

Milly, P. C. D., Moisture and heat transport in hysteretic, inhomogeneous porous media: A matric head-based formulation and a numerical model, *Water Resour. Res., 18*, 489–498, 1982.

Milly, P. C. D., A simulation analysis of thermal effects on evaporation from soil, *Water Resour. Res., 20*, 1087–1098, 1984.

Milly, P. C. D., A mass-conservative procedure for time-stepping in models of unsaturated flow, *Adv. Water Resour., 8*, 32–36, 1985.

Milly, P. C. D., and P. S. Eagleson, The coupled transport of water and heat in a vertical soil column under atmospheric excitation, *Rep. 258*, 234 pp., Ralph M. Parsons Lab., Mass. Inst. Technol., Cambridge, 1980.

Milly, P. C. D., and P. S. Eagleson, Parameterization of moisture and heat fluxes across the land surface for use in atmospheric general circulation models, *Rep. 279*, 226 pp., Ralph M. Parsons Lab., Mass. Inst. Technol., Cambridge, 1982.

Mualem, Y., A conceptual model of hysteresis, *Water Resour. Res., 10*, 514–520, 1974.

Mualem, Y., A new model for predicting the hydraulic conductivity

of unsaturated porous media, *Water Resour. Res.*, *12*, 513–521, 1976.

Mualem, Y., Extension of the similarity hypothesis used for modeling the soil water characteristics, *Water Resour. Res.*, *13*, 773–780, 1977.

Nimmo, J. R., and E. E. Miller, The temperature dependence of isothermal moisture vs. potential characteristics of soils, *Soil Sci. Soc. Am. J.*, *50*, 1105–1113, 1986.

Philip, J. R., and D. A. de Vries, Moisture movement in porous materials under temperature gradients, *Eos Trans. AGU*, *38*, 222–232, 1957.

Pruess, K., TOUGH user's guide, *Rep. NUREG/CR-4645*, 78 pp., U.S. Nucl. Reg. Comm., Washington, D. C., 1987.

Rose, C. W., Water transport in soil with a daily temperature wave, I, Theory and experiment, *Aust. J. Soil Res.*, *6*, 31–44, 1968.

Scanlon, B. R., Evaluation of liquid and vapor flow in desert soils based on chlorine 36 and tritium tracers and nonisothermal flow simulations, *Water Resour. Res.*, *28*, 285–297, 1992a.

Scanlon, B. R., Moisture and solute flux along preferred pathways characterized by fissured sediments in desert soils, *J. Contam. Hydrol.*, *10*, 19–46, 1992b.

Scanlon, B. R., Water and heat fluxes in desert soils, 1, Field studies, *Water Resour. Res.*, this issue.

Scanlon, B. R., F. P. Wang, and B. C. Richter, Field studies and numerical modeling of unsaturated flow in the Chihuahuan Desert, Texas, *Rep. Invest. 199*, 55 pp., Bur. Econ. Geol., Univ. of Tex., Austin, 1991.

Sophocleous, M., Analysis of water and heat flow in unsaturated-saturated porous media, *Water Resour. Res.*, *15*, 1195–1206, 1979.

van de Griend, A. A., P. J. Camillo, and R. J. Gurney, Discrimination of soil physical parameters, thermal inertia, and soil moisture from diurnal surface temperature fluctuations, *Water Resour. Res.*, *21*, 997–1009, 1985.

Wilkinson, G. E., and A. Klute, The temperature effect on the equilibrium energy status of water held by porous media, *Soil Sci. Soc. Am. Proc.*, *26*, 326–329, 1962.

P. C. D. Milly, U.S. Geological Survey, Geophysical Fluid Dynamics Laboratory/NOAA, P. O. Box 308, Princeton, NJ 08542.

B. R. Scanlon, Bureau of Economic Geology, The University of Texas at Austin, University Station, Box X, Austin, TX 78713.

(Received May 17, 1993; revised October 27, 1993; accepted November 15, 1993.)